Oxford Textbook of Neuroimaging

Edited by Massimo Filippi

Publisher: Oxford University Press
Print ISBN-13: 9780199664092
DOI: 10.1093/med/9780199664092.001.0001

Print Publication Date: Oct 2015
Published online: Oct 2015

Principles of brain single-photon emission computed tomography imaging

Chapter: Principles of brain single-photon emission computed tomography imaging
Author(s): Yong Du and Habib Zaidi
DOI: 10.1093/med/9780199664092.003.0008

Introduction

The historical development of medical imaging is marked by numerous significant technological accomplishments, driven by an unprecedented collaboration between multidisciplinary research groups. The first medical applications of tomographic imaging focused on the brain [1]. X-ray computed tomography (CT) and magnetic resonance imaging (MRI) have, for a long time, been the most widely-used imaging modalities for anatomic assessment of pathologic processes affecting the brain. Alternatively, radionuclide imaging methods, including single-photon emission computed tomography (SPECT) and positron emission tomography (PET) have emerged as useful medical imaging technologies for evaluating brain function. The development of the former technology for brain imaging dates back to 1976 when Drs Keyes and Jaszczak reported independently on the development of a brain SPECT system based on Anger camera mounted on a rotating gantry [2,3]. As nuclear medicine imaging has become integrated into clinical practice, several design trends have developed; with systems now available with a spectrum of features, from those designed for

clinical whole-body applications to others designed specifically for very high-resolution brain research applications [4].

SPECT is a non-invasive 3D tomographic imaging modality that is widely used in both clinical diagnosis and academic research to assess many diseases [5,6,7]. In SPECT imaging, the 3D distribution of a radionuclide-labelled agent administered to a patient is measured by detecting the gamma-photons emitted from the decay of the radioactive isotopes attached to the radiotracer. Because SPECT agents can be designed to target specific physiological functions, SPECT images can provide information on physiological and physiopathological processes at a molecular level. This unique feature makes it a useful tool for *in vivo* imaging of human brain function, especially for studying dysfunction of the neurotransmission system that is related to many brain diseases [8]. As a result, brain SPECT imaging became a powerful tool for diagnosis, prognosis, evaluation of response to therapy, and choice of treatment plan for many neurodegenerative diseases [9,10].

Brain single-photon emission computed tomography instrumentation

Conventional SPECT imaging systems

Since the purpose of SPECT imaging is to measure and represent the 3D distribution of the radiopharmaceuticals administered to the patient, the energies of gamma ray photons emitted by labelling radionuclides are high enough to allow penetration through the patient's body. The emitted photons can be detected using the so-called gamma camera (Fig. **8.1**) to generate a two-dimensional (2D) snapshot planar image. The 2D planar image is referred to as projection image since it represents a projected view of the three-dimensional (3D) radiotracer distribution at a certain angle. To acquire a 3D distribution, a series of projection images are taken around the patient at different discrete angles by rotating the gamma camera around the patient along the superior-inferior axis. After acquisition, the 3D distribution can then be reconstructed from the measured projection images using one of the available reconstruction techniques.

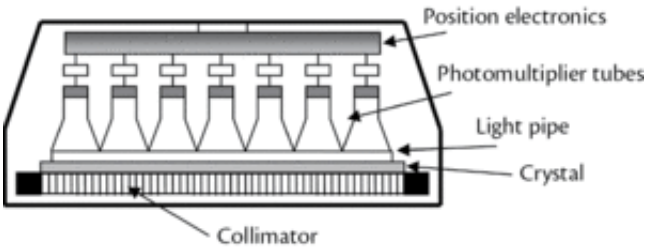

Fig. 8.1
Schematic representation of a SPECT gamma camera and its main components.

Usually, conventional SPECT imaging systems have two or three gamma cameras that are mounted on a gantry which provides mechanical support and rotation of the cameras. The main components of a gamma camera include the collimator, scintillation crystal, and photomultiplier tubes (PMTs) (Fig. **8.1**).

The collimator is used to selectively detect photons travelling in a certain direction because this information is needed for image reconstruction. It is made of highly dense photon absorbing

material, usually lead or tungsten, with a pattern of holes that allows only photons travelling parallel to the hole-direction to pass and reach the detector crystal. The holes can be arranged with the same direction (parallel hole collimator) or converge to certain points (for example, a cone beam collimator). The scintillator crystal, commonly sodium iodide (NaI) crystal, will absorb the photon and transfer its energy into visible or ultraviolet (UV) light photons through a process called scintillation. The number of visible or UV photons is proportional to the energy of incident photons. The visible/UV photons will travel to the PMT trough a light guide and produce an electric current signal. The PMT can multiply the current signal by a factor of as much as a million. The signal will then be further amplified through the amplifier and sent to processing electronics to generate the position and the energy information of the incident gamma photon. The information will then be passed on to an acquisition board/computer to generate the projection images.

Many of the clinical SPECT systems commercially available today are dual-modality SPECT/CT systems that also include a CT subsystem [11]. The SPECT images and CT images are complimentary to each other: SPECT images provide functional information, while the CT images provide anatomical information about location of disease site. By fusing the two images together, an accurate interpretation of images can be achieved. In addition, CT images can also be converted into attenuation maps required for attenuation compensation to improve SPECT image quality and quantitative accuracy. A plethora of CT scanners are used on combined SPECT/CT systems. Some use diagnostic quality CT to provide images suitable for clinical usage. To reduce patient radiation dose, low-dose CT scanners have also been deployed, mostly for typical nuclear medicine applications [12]. The image quality of low-dose CT is usually low and can only be used for attenuation compensation and localization. However, with the advance of iterative CT reconstruction algorithms, low-dose CTs can now also provide images of good quality [13].

Dedicated collimators and hardware for brain imaging

Most clinical SPECT systems can be used for various applications through appropriate selection of the most suited collimator for a particular study. The collimator is the most important part of a SPECT camera and is considered to be the main component affecting spatial resolution, sensitivity, and image noise. The choice of the collimator depends on the imaged object and trade-off considerations between sensitivity and spatial resolution. Usually, collimators with better spatial resolution have lower sensitivity, thus requiring a long acquisition time as otherwise the image will be very noisy. On the other hand, collimators with higher sensitivity will provide images with lower resolution. The most commonly used collimators are parallel-hole collimators. For example, in brain imaging using ^{99m}Tc-labelled compounds, a low-energy high-resolution (LEHR) parallel-hole collimator is often used to provide images with high spatial resolution. Because high spatial resolution is desirable in brain SPECT imaging, much worthwhile research focused on designing dedicated collimators to improve spatial resolution without sacrificing sensitivity [4].

Most of these collimators are converging collimators, in which the holes are focused to a line (fan beam collimator) or a point (cone beam collimator) in front of the collimator. A number of varying focal length collimators, where the holes are focused to different points in space have also been developed and evaluated in clinical setting. The detection efficiency of converging beam collimators is higher than that of parallel-hole collimators. The spatial resolution is also slightly better. Pinhole collimators have also been designed for imaging small organs, such as the thyroid or the extremities to provide a better spatial resolution, but at the expense of detection efficiency. The efficiency can be substantially improved by using multiple pinholes [14].

Furthermore, even in the presence of high count statistics, the mechanical motions involved and the bulk of the detector heads limit the shortest time in which a complete set of projections can be recorded [15,16]. Numerous attempts have been carried out to considerably boost brain SPECT sensitivity using several detector heads or ring-like arrangement of detectors to enable the very rapid acquisition of a full set of projections. Although the use of such dedicated systems is not prevalent in the clinic for brain SPECT imaging, they are useful for research applications and could also be useful for the assessment of the potential role of advances in instrumentation in the future [17,18]. A good example of full ring detector systems is the FASTSPECT, developed at the University of Arizona, which consists of 24 position-sensitive NaI(Tl) detectors that are completely stationary, together with a stationary set of 2-mm pinhole collimators, hence, achieving high sensitivity (fast dynamic brain scans) and high spatial resolution [19]. The ring detectors from stationary systems surround the head, which makes it possible to acquire data from 360° at the same time. This is especially attractive for dynamic imaging where a short repeat-scan over a period of time is performed. Another dedicated brain scanner with stationary annular NaI(Tl) detector is the CERASPECT system, developed by Digital Scintigraphics Inc. [20], which is equipped with a rotating collimator. A modified version of this collimator is the SensOgrade, a variable focusing collimator, which samples the projections unequally, with central regions more heavily represented to compensate for attenuation from central brain structures, thus yielding a four- to nine-fold increase in sensitivity compared with conventional dual-head cameras [21]. A third example is the SPRINT II system developed at the University of Michigan, which consists of 11 detectors arranged in a polygonal fashion and a rotating collimator, which allows the acquisition of a complete set of fan-beam projection data within 1/12 of a rotation [22]. Another example of unconventional systems is the NeuroFocus™ multi-cone beam imager (Neurophysics Corporation, Shirley, MA, USA), which produces tomographic SPECT images with an intrinsic spatial resolution of ~3 mm. The operation of the NeuroFocus™ high-definition focusing emission tomographic scanner (HDFET) follows the same principles of scanning optical microscopes to obtain high-resolution 3D images of biological tissue [23]. A highly focused point of light is scanned mechanically in three-dimensions to uniformly sample the volume under observation. As an alternative to dynamic SPECT imaging using multiple, fast rotations, strategies involving the use of only a single, slow camera rotation have been proposed [24,25]. Further advances in electronics are permitting new counting strategies and advances in electronic component capability are allowing for enhanced sensitivity [26].

Data acquisition protocols

Data acquisition

During SPECT image acquisition, a series of 2D projection images are taken at different angles by rotating the camera around the patient. To acquire enough data for image reconstruction, it is important to select the correct scan arc, which defines the range of rotation and where to start. For example, for cardiac imaging a 180° rotation from right posterior oblique to left anterior oblique is used, while for brain imaging a 360° rotation is usually required. One also needs to decide the orbit to specify the distance of the camera from the patient at each angle. The orbit can be either circular or non-circular. Non-circular means that the distances of the camera from the centre of rotation, termed as the radius of rotation, are not the same for different angles. In a circular orbit, the radius of rotation is constant. For a parallel-hole collimator, the closer the patient to the camera, the better the spatial resolution is. Therefore, a non-circular orbit is often used for imaging the torso, where the camera is positioned as close to the patient as possible. In modern SPECT

systems, this can be done automatically using optical sensors installed on the camera. For brain imaging, due to the round shape of the head, a circular orbit is often used where the operator can specify the radius of rotation.

The gamma photons emitted from radioactive decay have characteristic energy/energies, called peaks that are specific to the isotope. For example, ^{99m}Tc decay emits gamma photons at 140.5 keV only, while ^{123}I decay emits gamma radiation mainly at 159 keV with some other higher energy peaks with low abundance. Ideally, during SPECT imaging only photons detected with the exact peak energy will be counted as true events. However, due to the limited energy resolution of the gamma camera, the energies of detected photons are Gaussian distributed around the peak energy. To maintain a reasonable sensitivity, photons detected with energies in a certain range around the peak energy will all be counted as true events. This energy range is called the acquisition energy window. On the other hand, photons scattered in the patient body will contaminate the images and they usually have a broad energy distribution lower than the peak. To reduce the number of recorded scattered photons, the energy window should not be too wide. The choice of the energy window is dictated by a balance between recording as many peak photons as possible without significantly increasing scattered photon counts. Commonly-used energies windows are usually 15–20% wide and centred around the peak energy.

Another important parameter in SPECT is the acquisition time for each projection angle. Long acquisition times result in high counts and low image noise. However, this will also reduce patient comfort and increase chances of artefacts caused by patient movement during acquisition. Overall, the choice of scanning parameters depends on the imaging task at hand. The aim is to acquire as much complete data as possible to provide good image quality and make the process comfortable to patients. Most commercial SPECT systems have manufacturer preset or recommended acquisition protocols for common applications, such as cardiac imaging, brain imaging, tumour imaging, and bone scans. New protocols can also be set by the users to accomplish their special needs. This requires the availability of a qualified medical physicist having the required skills, expertise, and knowledge of this technology.

Dual-isotope imaging

In some situations, it may be necessary to acquire images of more than one physiological function to provide accurate diagnosis. For example, in brain imaging of the dopaminergic system, it is generally recognized that the analysis of the integrity of both the pre- and the post-synaptic neuron is crucial in distinguishing different parkinsonian syndromes. The presynaptic neurons can be imaged with an agent targeting the dopamine transporter (DAT) on the cell membrane. Agents targeting the dopamine receptors, especially type II receptor (D2R), could be used in imaging the post-synaptic neurons [27,28]. Traditionally, DAT and D2R imaging are performed on different days because most of DAT and D2R agents are labelled with the same isotope (^{123}I). Since the half-life of ^{123}I decay is 13 hours, the two scans must be separated by several days to allow the radioactivity from the first scan to decay in order to avoid contamination of the second scan. During this interval, the patient's physiological status may have changed. Moreover, the patient's position during the two scans will probably be different, which will cause registration errors between the images [29]. This is particularly relevant for patients suffering tremors, where the artefacts in the two images may have different patterns that will further complicate diagnosis.

These drawbacks can, however, be overcome by using simultaneous dual-isotope acquisition

methods. Taking advantage of modern cameras' higher energy resolution and the ability to acquire multiple energy windows, simultaneous dual-isotope imaging is a method that can be used to diagnose diseases by imaging different physiological information revealed by agents labelled with different isotopes that emit gamma photons at different energies. Compared to separate imaging, simultaneous acquisition reduces acquisition time, patient discomfort and motion artefacts. Perhaps, more importantly, simultaneous acquisition ensures perfect registration of the images from both isotopes in time and space. Furthermore, motion artefacts, if any, will be the same on images of both isotopes. For example, with the introduction of ^{99m}Tc-labelled DAT ligands, such as ^{99m}Tc-TRODAT, SPECT imaging of the DAT and D2R can now be carried out simultaneously using dual-isotope ^{99m}Tc/^{123}I imaging. There is also interest in simultaneous imaging of brain perfusion using ^{99m}Tc-HMPAO and neurotransmission with ^{123}I-IBZM. However, research on simultaneous ^{99m}Tc/^{123}I dual-isotope brain imaging has shown that image quality is significantly degraded by the cross-talk contamination between the two isotopes. Cross-talk here refers to the contamination of one agent/isotope's image caused by the other isotope used in simultaneous dual-isotope imaging. Before simultaneous imaging can be adopted clinically, an efficient cross-talk compensation method must be developed and validated [30,31,32].

Image reconstruction

Image reconstruction techniques

SPECT image formation can be expressed as an integration of the 3D radioactivity distribution along each projection direction, i.e. line of integration, into a series of 2D data. Image reconstruction is an inverse problem that tries to estimate the 3D activity distribution from the 2D projection data. Both analytical and iterative reconstruction approaches have been devised to solve this reconstruction problem in order to provide the best estimates that are as close to the truth as possible. These two categories of reconstruction strategies are briefly summarized.

Analytical reconstruction

As described above, a projection is an integration of the activity distribution along the line of integration. The collection of these projections as a function of projection angle is referred to as the Radon transform of the object [33]. By inversing the radon transform of the projections, the original 3D activity distribution can then be reconstructed analytically. The most widely used analytical reconstruction method is the filtered back-projection (FBP) algorithm, which is still used in many image reconstruction tasks.

Analytical reconstruction methods, such as FBP, focus on the geometry and simplify the physics. They are simple, fast, and can provide accurate results when the assumed projection model matches the image formation process. However, they are sensitive to noise and missing data, which will result in artefacts and loss of reconstructed image resolution. Another major disadvantage of analytical methods is that they do not allow precise modelling of the physical and statistical characteristics of the data acquisition process, thus resulting in image artefacts and poor quantitation. This problem can, however, be solved through the use of iterative reconstruction algorithms, where image degrading factors can be modelled during the reconstruction as described in the next section.

Iterative reconstruction

Fig. **8.2** shows a generalized flow chart of an iterative reconstruction algorithm. An iterative method can be regarded as an operator working between the image space, i.e. the 3D space representing the activity distribution in the object, and projection space, which represents the SPECT measurement of the 2D projections. In an iterative method, an initial estimate is projected to generate an estimated projection of the current estimate. Estimated projections are then compared with the measured projections. The error between the two is back-projected to the image space, then used to update the current estimate. By repeating the projection–back-projection process in a feedback loop to update the image estimate until a given criterion is fulfilled, iterative methods can produce high-quality images with improved resolution and noise properties, and result in adequate quantitative accuracy.

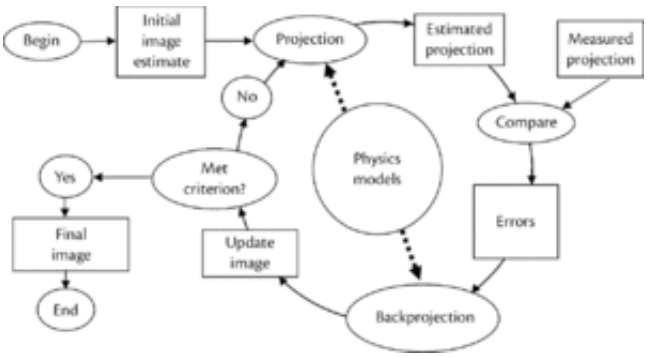

Fig. 8.2
Flow chart of an iterative reconstruction algorithm.

Among all iterative reconstruction algorithms, the most successful and popular ones are statistical reconstructions, which are often simply referred to as iterative reconstruction approaches. An iterative statistical reconstruction method consists of three major components:

1. An underlying statistical model with associated objective function.
2. An iterative algorithm to find the optimal estimate in terms of the objective function.
3. A model of the image formation process often implemented using a projector–back-projector pair.

Among these, the projector–back-projector pair is very important. It serves as a bridge connecting the image space (estimate) and the projection space (measurement). It is in the projection–back-projection operators that the exact modelling of the physics and image formation process is performed. Through the iterative process, the modelling allows for the compensation of image-degrading factors, such as scatter and attenuation. The underlying statistical model and resulting objective function play the role of deciding how well the estimate matches the projections, taking into account the noise properties of the measured data and knowledge about the characteristics of the underlying activity distribution.

The most popular iterative reconstruction algorithm in SPECT is the maximum-likelihood expectation-maximization (ML-EM) algorithm and its accelerated variation, the ordered-subsets expectation-maximization (OS-EM) approach [34,35]. The ML-EM algorithm is based on the fact that photon emission and detection from radioactive decay are Poisson distributed. It attempts to maximize the statistical likelihood that the measured projections came from the reconstructed

image. In OS-EM, the algorithm is made faster by using only part of the projection data, called a subset, during each update. Compared with ML-EM, OS-EM converges faster with a factor approximately equal to the number of subsets used. This category of reconstruction strategies was so successful that most current SPECT systems offer software for end users to perform ML-EM and OS-EM reconstruction with various physics modelling options. While this has been shown to be of great practical value, it should be noted that OS-EM has a relatively weak theoretical basis and its convergence properties are only poorly understood.

Despite their advantages and attractive properties, these technical advances have many limitations. Iterative methods can be very computationally demanding, particularly when complex models are used to model the physics of the image formation process. However, the widespread availability of high performance computing, even on desktop computers (including graphics processing unit and cloud computing), and the continuing development of rapidly converging algorithms has led to renewed interest in iterative techniques and made them a hot topic for leading manufacturers and academic research groups.

Image degrading factors

Ideally, only photons with an original path that is along the collimator hole direction can be detected in the projections. However, when gamma-photons travel inside an object, they interact with matter through a number of physical processes, such as photoelectric absorption and Compton scatter [36]. The probability of occurrence of each process depends on the energy of the photon and the electron density of the material. Those interactions could reduce the number of photons or change a photon's path and energy. The detection of those alternated photons can cause false information and degrade the image quality in multiple ways. Fig. **8.3** demonstrates the different factors that can degrade SPECT images. Among those, the most significant factors are photon attenuation, scatter, and collimator-detector response.

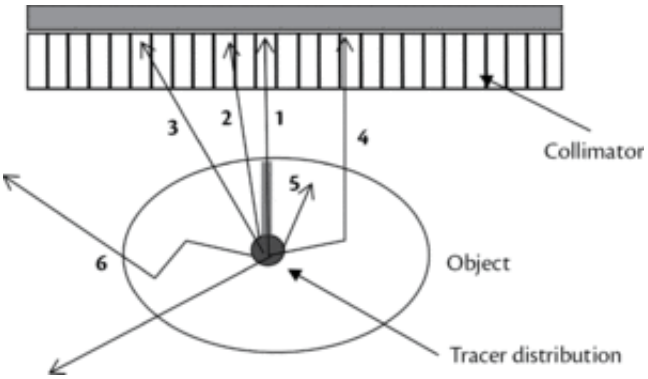

Fig. 8.3
Overview of photon detection in SPECT representing different physical degrading factors. (1 and 2) Photons pass through the collimator without interactions, 1 also shows the attenuation of the photon intensity. (3) Photon penetrates or scatters in the collimator-detector system. (4) Photon scatters inside the imaging object. (5) Photoelectric absorption; and (6) Photon escapes the object without hitting the collimator-detector system.

When photons pass through the imaging object, they can be absorbed by photoelectric absorption

or diverted by Compton scatter. As a result, the intensity of the photon flux finally reaching the detector will be much smaller compared with the original one and this effect is referred to as photon attenuation. Attenuation reduces the measured projection counts. The degree depends on the photon path and the object. It can be expressed as an exponent function of the product of the attenuation coefficient of the object and the distance the photon has to travel in the object. If not compensated for, attenuation leads to reconstructed images with reduced intensity in voxels deep in the object. It can also result in visible artefacts and quantification with significant errors.

A number of photons emitted from the radionuclide will scatter in the patient at least once before exiting the body. The dominant scatter events are Compton scatter, which reflects a collision interaction between a gamma-photon and an outer shell electron of an atom. During the collision, gamma-photons will transfer some of their energy to the electron and change the direction of movement. The energy of the scattered photon is a function of the scattering angle, given by the Compton formula. The photon loses most of its energy when it is scattered backward (180°). When the scattering angle decreases, the energy of the scattered photon comes close to the incoming photon's energy. The probability of Compton scattering depends on the photon energy and the number of electrons available in the object. The probability of the angular distribution of the scattered photon, described by Klein–Nishina formula, is also a function of the photon energy and scattering angle [36].

Because Compton scattering reduces photon energy, usually only those photons scattered once or twice, and within a small scattering angle can be detected within the imaging energy window. Since scatter diverts the direction of scattered photons, when those photons are detected, they result in counts in voxels that they would not reach without being scattered. Scatter in projection data is spatially varying and is a function of the object attenuation properties, the imaging energy window, and the source distribution. In brain imaging using ^{123}I- or ^{99m}Tc-labelled compounds, scattered photons can contribute up to 11% of the total counts in the final images. If not compensated for, scatter could result in a structured background artefact that resembles the medium- and low-frequency character of the activity distribution, and as such reduces image contrast. Quantitatively, scatter can lead to overestimation of tracer uptake [37,38].

The collimator is the crucial element determining the sensitivity, spatial resolution and contrast of SPECT images. A perfect collimator only allows the detection of photons that travel in a direction parallel to the collimator hole. As shown in Figs **8.3** and **8.4**, since a real collimator hole has a finite geometric size, photons incident within a small acceptance angle from the hole-direction can still be detected. This is referred to as geometrically-collimated photons or collimator geometric response. In addition, due to statistic variations, the position of photon absorption in the crystal is usually determined with imprecision, and is defined as intrinsic resolution. Both collimator geometric response and intrinsic resolution reduce the spatial resolution and cause blurring of the image. These effects can be modelled using geometric response functions. Typically, Gaussian functions are used to analytically model the geometric responses. The full width at half maximum of the Gaussian is, therefore, often used as an indication of the system spatial resolution [39]. In general, collimators with large holes allow more photons to pass through, but will also cause more spatial blurring. Collimators with small holes can provide better spatial resolution, but lower sensitivity. The resolution is also a function of distance: the farther the object from the collimator, the worse the resolution.

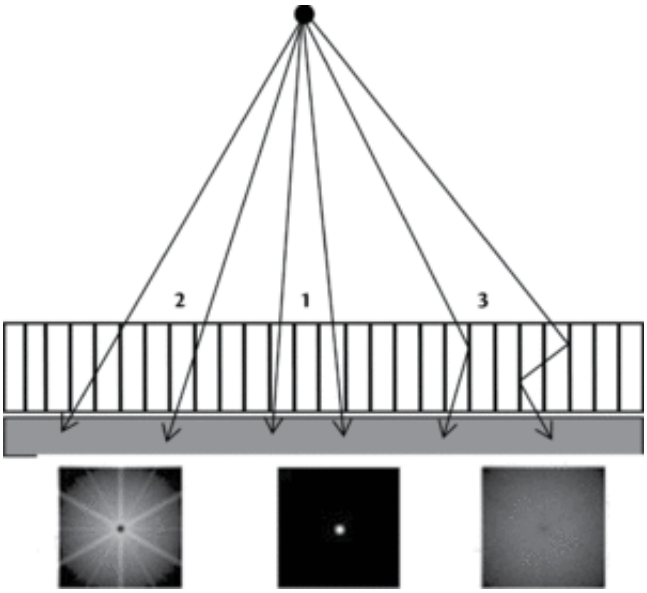

Fig. 8.4
Different components of the collimator-detector response. (1) Geometric response. (2) Collimator penetration. (3) Collimator scatter.

Photons incident on the collimator with large angles are usually absorbed by the septa between collimator holes. However, some high-energy photons emitted from isotopes such as ^{123}I can still penetrate the septa or pass through after scattering inside the septa as shown in Fig. **8.4**. The penetrated photons from a point source usually result in a star- or stripe-shaped pattern in the projection. Collimator scattered photons usually result in a broadly distributed background in the projection. If not compensated for, these photons can cause artefacts in the reconstructed images. The full collimator-detector response, including geometric response, collimator penetration, and collimator scatter depends on the collimator geometry and the photon energy. It can be modelled by the collimator-detector response function (CDRF) that is measured or simulated by placing a point source at various distances from the face of the collimator.

Fig. **8.5** shows simulated SPECT images considering the different image degrading factors discussed above. The images were reconstructed using FBP without post-reconstruction filtering. From left to right, the image quality is getting worse because more degrading factors were included in the simulation process. The worst image is the last one on the right, which includes all the physical degrading factors and is the most representative of what is found in the clinic without any compensation. The images also indicate that attenuation reduces the intensity at the centre of the brain, collimator-detector response blurs images and reduces spatial resolution, and scatter reduces image contrast.

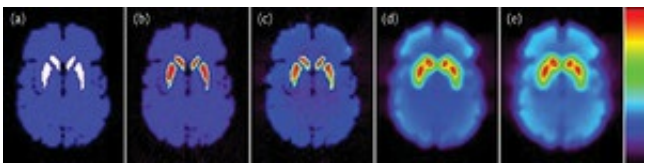

Fig. 8.5

Effects of image degrading factors. The images represent the actual tracer distribution in the striatal brain phantom (a) and reconstructed SPECT images generated without degrading factors (b); with photon attenuation (c); with attenuation and collimator-detector response blurring (d); and with attenuation, collimator-detector response blurring, and scatter (e).

The spatial resolution in typical SPECT images is around 1–2 cm. As shown in Fig. **8.5**, the finite spatial resolution results in blurred images with partial volume effects (PVEs). PVEs include both a loss of counts in structures smaller than two or three times the system resolution's full width at half maximum (partial volume) and contamination between adjacent regions (spillover). PVEs also depend on the shape, size, and relative activities of the objects of interest. The procedures applied after image acquisition, such as image reconstruction, will also affect the level of PVEs. In brain imaging, due to the fine dimensions of the structures of interest, such as the putamen and caudate, PVEs can cause large quantitative errors.

In addition, SPECT images also suffer from noise. Noise in SPECT images consists mainly of statistical noise resulting from the random nature of photon emission (following radioactive decay) and detection processes. It can be characterized by a Poisson distribution in which the variance equals the mean. Therefore, noise in SPECT data is a function of the number of detected counts—the higher the counts, the lesser the noise. Noise could significantly affect image quality and quantitative accuracy, and reduce the detectability of subtle abnormalities and their measurement. Noise can also cause image artefacts, introducing textures into uniformly-distributed regions. Increasing the count level using long acquisition times or high injection doses can reduce noise. Low pass filtering is often used to smooth out noise in the reconstructed images. Alternatively, constrains can also be applied during iterative reconstruction to reduce noise.

Cross-talk in dual-isotope imaging

In simultaneous dual-isotope imaging, a photon emitted from one isotope can be detected in another isotope's energy window owing to the finite energy resolution of the detector system, and the interaction of photons with the object and collimator-detector system. These photons can reduce image quality, degrade quantitative accuracy, and cause artefacts in the images. This effect is referred to as cross-talk contamination. Cross-talk contamination depends on the emission energies and the imaging energy windows of both isotopes. As such, the overall impact is different for various isotope combinations, making it difficult to find a universal compensation method.

Fig. **8.6** shows simulated energy spectra of a simultaneous ^{99m}Tc/^{123}I dual-isotope brain SPECT study. The spectra indicate that cross-talk from ^{99m}Tc into ^{123}I projection data originates mainly from unscattered ^{99m}Tc photons that are detected in the ^{123}I energy window as a result of the detector's finite energy resolution. The cross-talk from ^{123}I into ^{99m}Tc window, however, is complex and includes photons originating from a variety of processes. In addition to the 159 keV photons used for imaging, ^{123}I decay also emits high-energy photons with energies ranging from 182 keV to 783 keV with a total abundance of ~3% [40]. The down-scatter of these photons into both ^{99m}Tc and ^{123}I energy windows can further contaminate the images of both radionuclides.

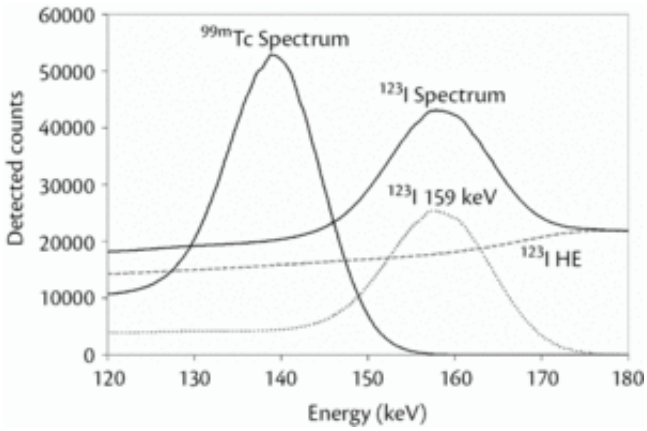

Fig. 8.6
Simulated energy spectra of a ^{99m}Tc/^{123}I dual-isotope study.

Compensation techniques

To improve image quality and quantitative accuracy, imaging degrading factors have to be compensated for. To compensate for attenuation, an attenuation map representing the spatial distribution of the patient's attenuation coefficients is required. The attenuation map can be derived by scanning the patient using either transmission sources of radionuclides having an energy close to the energy of the radionuclide used for SPECT imaging or from CT images acquired on combined SPECT-CT systems. In the past, analytical methods have been used to compensate for photon attenuation, which usually involves scaling the projection image or post-reconstruction filtering [41,42]. Because these methods often assume uniform attenuation of the medium, they can only provide an approximate compensation, and sometimes may even cause more artefacts when the object is non-homogeneous [43].

Accurate attenuation compensation can be achieved using iterative reconstruction-based compensation, where the attenuation map acquired from a transmission scan is used to model the attenuation in the projection–back-projection operators [44]. Iterative reconstruction-based attenuation compensation has been shown to significantly improve the image quality and quantitative accuracy, and is currently widely used in the clinic. Similarly, an accurate compensation of the collimator-detector response is usually achieved through iterative reconstruction-based compensation by including the CDRF models in the projection–back-projection operators [45].

Compton scatter compensation strategies can be categorized into methods that compensate for scatter directly on the projection data (pre-reconstruction), methods that compensate for scatter during the reconstruction process and post-reconstruction restoration filtering [38]. Methods that operate on projection data usually accomplish the compensation by subtracting the scatter estimate from measured projection data. Scatter is often estimated by scaling projection data acquired in one or two scatter windows with pre-determined factors [46,47,48]. The scatter can also be estimated by analysing the spectrum of projection data acquired in multiple narrow (1–4 keV wide) energy windows using spectral fitting techniques or artificial neural networks [49,50]. Post-reconstruction filtering usually compensates for the scatter by deconvolving the reconstructed images with a scatter response function (ScRF) acquired through experimental measurements or derived from Monte Carlo simulations [51]. Both pre- and post-reconstruction scatter compensation methods

make simple assumptions about the scatter component, such as shift-invariance, which results in biased scatter estimates. Furthermore, scatter compensation is achieved by subtraction of the estimated scatter component, which is usually accompanied by a large increase in statistical noise [52,53].

Reconstruction-based scatter compensation (RBSC) methods compensate for scatter by modelling the spatially varying and object-dependent SRF in the projection–back-projection operators within the framework of an iterative reconstruction algorithm [37,54]. RBSC methods were shown to provide the most accurate scatter compensation among all methods [37,38]. Currently available scatter modelling techniques for RBSC include the slab-derived scatter estimation (SDSE) model, the effective source scatter estimation (ESSE) techniques [54,55], the non-stochastic numerical integration method [56,57], and the fast Monte Carlo simulation approach [58,59].

To demonstrate the efficacy of the various image correction techniques, Fig. **8.7** shows representative SPECT brain images reconstructed with compensation for various degrading factors. The image quality gradually improves when more degrading factors are compensated for. The best result is achieved by including compensations for all the physical degrading factors.

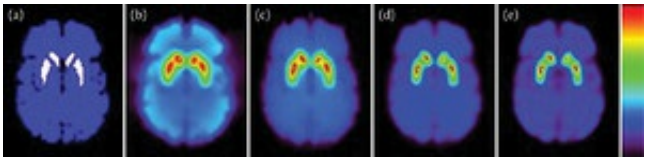

Fig. 8.7
Images reconstructed with compensation for different physical degrading factors. The images represent the actual tracer distribution in the striatal brain phantom (a) and reconstructed SPECT images obtained without compensation (b); with attenuation compensation (c); with attenuation and collimator-detector response compensation (d); and with attenuation, collimator-detector response, and scatter compensation (e).

Most of cross-talk compensation methods have been developed based on scatter compensation methods [60,61,62,63,64,65]. The procedures include estimating the cross-talk, and subtracting it prior to reconstruction or using reconstruction-based compensation approaches. The cross-talk can be estimated using multiple energy window methods, including the triple-energy window technique or more complicated techniques, such as those using artificial neural networks, constrained spectral deconvolution, and principal component analysis. Cross-talk models were also developed for iterative reconstruction-based compensation that use estimates of the activity distribution for each isotope combined with the physics of the image-formation process to estimate the cross-talk. For example, model-based cross-talk compensation (MBCC) uses the ESSE technique to model photon interactions inside objects, and collimator-detector response functions to model photon interactions within the collimator-detector and the finite energy resolution of the detector [66]. Monte Carlo simulations have also been used for cross-talk estimation [58].

Fig. **8.8** shows simultaneous ^{99m}Tc/^{123}I dual-isotope images reconstructed without cross-talk compensation and with MBCC, compared with cross-talk free single-isotope images. Overall, without compensation, the cross-talk reduced image contrast for both ^{99m}Tc and ^{123}I images. After compensation using MBCC, the images are very close to single-isotope images, indicating the

efficacy of cross-talk compensation [66].

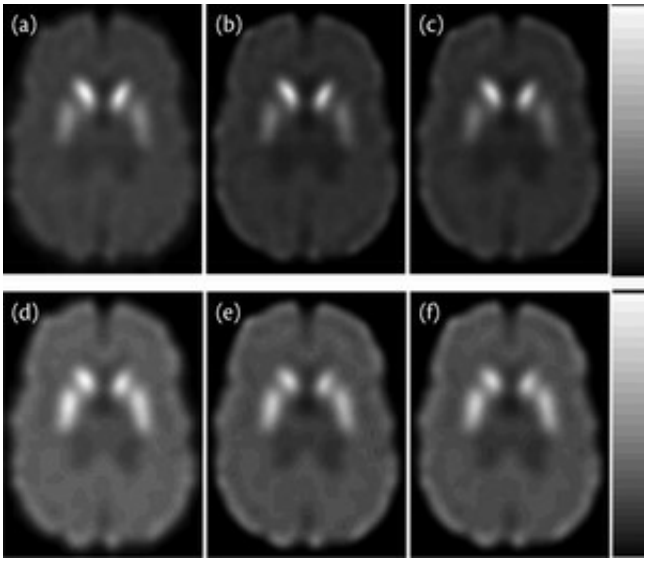

Fig. 8.8
Simultaneous dual-isotope images. Top row: ^{99m}Tc images, bottom row: ^{123}I images. Dual-isotope images without cross-talk compensation (a and d); with MBCC (b and e); and cross-talk free single-isotope images (c and f).

Compensation for collimator-detector response can improve image resolution and reduce PVEs. However, complete count recovery has not been achieved yet [45,66,67,68]. Additional partial volume effect compensation is usually required. A plethora of partial volume compensation (PVC) strategies have been proposed [69,70]. Some of these methods attempt to remove or reduce the PVEs by deconvolving the image with the system point spread function. To improve noise properties, regularization is required during deconvolution. Pixel-by-pixel template-based approaches, where spill-in and spill-out counts are modelled by their effect on template images followed by compensation using subtraction and division, were also proposed [71]. Alternative approaches directly compensate for PVEs at the regional level to provide corrected activity estimates using a transfer matrix of PVEs [72]. Application of PVC to dopaminergic neurotransmission SPECT imaging has been shown to significantly improve quantitative accuracy [73]. Reconstruction-based PVC methods have also been proposed, using for instance, the maximum a posteriori approach [74]. Methods that incorporate PVC directly into the kinetic modelling process by introducing additional parameters that model PVEs were also reported for dynamic imaging [75]. Overall, accurate PVC requires perfect knowledge of the system resolution and precise delineation of regions-of-interest (ROIs) boundaries, which can be performed through the use of registered high-resolution anatomical images such as CT or MRI.

Image quality assessment and data analysis

Qualitative versus quantitative

Traditionally, SPECT images have been qualitatively assessed by visual observation of tracer uptake

in regions linked to known patterns of various diseases. The visual assessment conveys information on whether the tracer uptake is normal or abnormal, and, if abnormal, it provides an idea about the magnitude of the abnormality. In brain SPECT, the visual assessment provides information about right to left asymmetries and which structures are the most affected by disease.

However, because the uptake of an imaging tracer is often strongly correlated to the integrity of physiological functions in targeted ROIs, the quantitative measurements of tracer uptake in those ROIs can provide more information for in-depth assessment. Most importantly, quantitative analysis enables to estimate physiological parameters, such as blood flow, metabolism, and receptor concentration. These measurements can be used in clinical diagnostic work-up or in the assessment of the efficacy of therapies. For instance, the binding of DAT or D2R agents in the dopaminergic system are strongly correlated to the degree of disease progression in movement disorders. Recent research has demonstrated that the quantitative measurement of tracer uptake can provide more information for better assessment of many brain disease processes [10,76,77].

Quantification techniques

Quantitative studies usually involve defining ROIs on the images and then measuring the trace uptake inside them. One commonly used method in brain SPECT is to calculate the specific binding potential (SBP, also called specific uptake value) of the radiotracer in the ROI as the ratio between activity concentration inside the ROI and the activity concentrations in a reference region that has no specific binding for the tracer considered. The images can also be assessed using more sophisticated voxel-based quantitative methods, such as statistical parametric mapping (SPM), which automatically maps brain regions to a standardized atlas and compares the images with a database of normal subjects [77]. Compared with SPM, computing the SBP greatly simplifies data analysis and often provides a reliable measurement.

Dynamic SPECT can also be used to acquire a series of images of tracer uptake within the ROI from the injection time till the time the tracer is washed out or the distribution reaches equilibrium. Consequential kinetic analysis of the acquired dynamic data using tissue compartment models provides unique information that improves the discrimination between healthy and diseased tissue compared with static images [25].

Future perspectives

The major challenge facing the future of brain SPECT imaging is the widespread adoption and availability of PET in clinical setting. PET has better spatial resolution and higher sensitivity than SPECT. To compete with PET, future brain SPECT systems should provide images with better quality and improved quantitative accuracy that is equivalent or at least comparable with PET.

Software

Software development in SPECT is currently focusing on improving image quality and quantitative accuracy of reconstructed images. This includes the development of novel reconstruction algorithms and image correction techniques. Promising results have been achieved using maximum a posteriori (MAP) reconstruction algorithms that incorporate anatomical knowledge into the SPECT reconstruction process. The anatomical information can be obtained from MR images, which are routinely performed in the clinic for brain studies. MRI provides detailed structural

information about the brain which is missing in SPECT. In MAP reconstruction, the anatomical information could be used as a prior to reduce statistical noise and improve the resolution, especially when anatomical region-based priors are used to reduce noise inside each structure but not across the boundaries [74,78,79]. Different priors can also be used for each structure based on its biological properties. Fig. **8.9** shows examples comparing OS-EM with MAP reconstructions using different regional priors. The OS-EM images contain a significant amount of noise. In the MAP reconstruction, a uniform prior was used for the striatum assuming uniform uptake. A smooth prior was used for the background to reduce noise. Images from MAP reconstruction portray much reduced noise and improved spatial resolution for the striatum compared with OS-EM reconstruction.

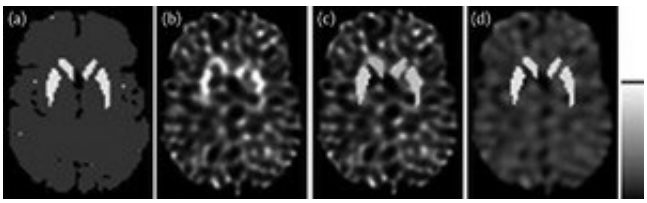

Fig. 8.9
Brain SPECT images reconstructed using different algorithms showing the actual tracer distribution in the striatal brain phantom (a). OS-EM reconstruction (b). MAP reconstruction with only a uniform prior for the striatum (c). MAP reconstruction with a smooth prior for background and a uniform prior for the striatum (d).

Hardware

A more fundamental way of improving SPECT images is to develop new detector technology that could provide images with high sensitivity and high spatial resolution. Detectors using semiconductor technology, where direct photon conversion detectors such as cadmium telluride are mostly used, acquire data at better energy resolution than conventional gamma cameras [80,81]. This could potentially provide images with less scatter and reduce cross-talk in dual-isotope imaging. Development in multimodality imaging is also being pursued. In SPECT/CT, recent developments in dual-energy CT scanners make it possible to segment soft tissues in CT images without the use of contrast agents. Simultaneous SPECT/MRI is also promising and should enable both MR and SPECT images of patient's brain to be acquired at the same time, thus providing perfectly registered images.

Acknowledgements

This work was supported by the Swiss National Science Foundation under grant SNSF 31003A-149957

References

1. Abraham T, Feng J. (2011). Evolution of brain imaging instrumentation. *Seminars in Nuclear Medicine*, **41**, 202–19.

2. Keyes J, Jr, Orlandea N, Heetderks W, et al. (1977). The Humongotron-a scintillation-camera transaxial tomograph. *Journal of Nuclear Medicine*, **18**, 381–7.

3. Jaszczak RJ, Murphy PH, Huard D, et al. (1977). Radionuclide emission computed tomography of the head with 99mTc and a scintillation camera. *Journal of Nuclear Medicine*, **18**, 373–80.

4. Accorsi R. (2008). Brain single-photon emission CT physics principles. *AJNR American Journal of Neuroradiol*ogy, **29**, 1247–56.

5. Jaszczak RJ. (2006). The early years of single photon emission computed tomography (SPECT): an anthology of selected reminiscences. *Physics in Medicine and Biology*, **51**, R99–115.

6. Madsen MT. (2007). Recent advances in SPECT imaging. *Journal of Nuclear Medicine*, **48**, 661–73.

7. Hutton BF. (2010). New SPECT technology: potential and challenges. *European Journal of Nuclear Medicine and Molecular Imaging*, **37**, 1883–6.

8. Camargo EE. (2001). Brain SPECT in neurology and psychiatry. *Journal of Nuclear Medicine*, **42**, 611–23.

9. Catafau AM. (2001). Brain SPECT of dopaminergic neurotransmission: a new tool with proved clinical impact. *Nuclear Medicine Communications*, **22**, 1059–60.

10. Devous MD. (2002). Functional brain imaging in the dementias: role in early detection, differential diagnosis, and longitudinal studies. *European Journal of Nuclear Medicine*, **29**, 1685–96.

11. Seo Y, Mari C, and Hasegawa BH. Technological development and advances in single-photon emission computed tomography/computed tomography. *Seminars in Nuclear Medicine*, **38**, 177–98.

12. Franc BL, Myers R, Pounds TR, et al. (2012). Clinical utility of SPECT-(low-dose)CT versus SPECT alone in patients presenting for bone scintigraphy. *Clinical Nuclear Medicine*, **37**, 26–34.

13. Beister M, Kolditz D, and Kalender WA. (2012). Iterative reconstruction methods in X-ray CT. *Physics in Medicine*, **28**, 94–108.

14. Beekman F, and van der Have F. (2007). The pinhole: gateway to ultra-high-resolution three-dimensional radionuclide imaging. *European Journal of Nuclear Medicine and Molecular Imaging*, **V34**, 151–61.

15. Cherry SR. (2004). In vivo molecular and genomic imaging: new challenges for imaging physics. *Physics in Medicine*, **49**, R13–48.

16. Meikle SR, Kench P, Kassiou M, et al. (2005). Small animal SPECT and its place in the matrix of molecular imaging technologies. *Physics in Medicine and Biology*, **2005**, 22.

17. Zaidi H, (ed.) (2006). *Quantitative analysis in nuclear medicine imaging*. New York: Springer 2006.

18. Zaidi H, and El Fakhri G. (2008). Is absolute quantification of dopaminergic neurotransmission studies with 123I SPECT ready for clinical use? *European Journal of Nuclear Medicine* and

Molecular Imaging, **35**, 1330–3.

19. Rowe RK, Aarsvold JN, Barrett HH, et al. (1993). A stationary hemispherical SPECT imager for three-dimensional brain imaging. *Journal of Nuclear Medicine*, **34**, 474–80.

20. Genna S, and Smith AP. (1988). The development of Aspect, an annular single-crystal brain camera for high-efficiency SPECT. *IEEE Transactions in Nuclear Sciences*, **35**, 654–8.

21. El Fakhri G, Ouyang J, Zimmerman RE, et al. (2006). Performance of a novel collimator for high-sensitivity brain SPECT. *Medical Physics*, **33**, 209–15.

22. Rogers WL, Clinthorne NH, Shao L, et al. (1988). SPRINT II: a second generation single photon ring tomograph. *IEEE Transactions in Nuclear Sciences*, **7**, 291–7.

23. Seibyl JP, Stobbart HA, Martin D, et al. (2002). Evaluation of high resolution NeuroFocus SPECT device for small animal imaging (abstract). *Journal of Nuclear Medicine*, **2002**, 43

24. Farncombe T, Celler A, Noll D, et al. (1999). Dynamic SPECT imaging using a single camera rotation (dSPECT). *IEEE Transactions in Nuclear Sciences*, **46**, 1055–61.

25. Gullberg GT, Reutter BW, Sitek A, et al. (2010). Dynamic single photon emission computed tomography-basic principles and cardiac applications. *Physics in Medicine and Biology*, **55**, R111–91.

26. Wong WH, Li H, Uribe J, et al. (2001). Feasibility of a high-speed gamma-camera design using the high-yield-pileup-event-recovery method. *Journal of Nuclear Medicine*, **42**, 624–32.

27. Acton PD, and Mozley PD. (1999). Single photon emission tomography imaging in parkinsonian disorders: a review. *Behavioural Neurology*, **12**, 11–27.

28. Tatsch K, Asenbaum S, Bartenstein P, et al. (2002). European association of nuclear medicine procedure guidelines for brain neurotransmission SPET using 123I-labelled dopamine transport ligands. *European Journal of Nuclear Medicine and Molecular Imaging*, **29**, BP30–5.

29. Djang DS, Janssen MJ, Bohnen N, et al. (2012). SNM practice guideline for dopamine transporter imaging with 123I-ioflupane SPECT 1.0. *Journal of Nuclear Medicine*, **53**, 154–63.

30. Devous MD, Lowe JL, Payne JK. (1992). Dual-isotope brain SPECT imaging with Technetium and I-123—Validation by phantom studies. *Journal of Nuclear Medicine*, **33**, 2030–5.

31. Devous MD, Payne JK, and Lowe JL. (1992). Dual-isotope brain SPECT imaging with Technetium and I-123—Clinical validation using Xe-133 SPECT. *Journal of Nuclear Medicine*, **33**, 1919–24.

32. Ivanovic M, Weber DA, Loncaric S, et al. (1994). Feasibility of dual radionuclide brain imaging with I-123 and Tc-99m. Medical Physics, **21**, 667–74.

33. Kak AC, and Slaney M. (1988). *Principles of computerized tomographic imaging*. IEEE Press.

34. Hudson HM, and Larkin RS. (1994). Accelerated image reconstruction using ordered subsets of projection data. *IEEE Transactions in Nuclear Sciences*, **13**, 601–9.

35. Lange K, and Carson R. (1984). EM reconstruction algorithms for emission and transmission tomography. *Journal of Computer Assisted Tomography*, **8**, 306–16.

36. Cherry SR, Sorenson JA, and Phelps ME. (2012). *Physics in nuclear medicine*, 4th edn. Philadelphia, PA: Elsevier Saunders.

37. Zaidi H, and Koral KF. (2004). Scatter modelling and compensation in emission tomography. *European Journal of Nuclear Medicine and Molecular Imaging*, **31**, 761–82.

38. Hutton BF, Buvat I, and Beekman FJ. (2011). Review and current status of SPECT scatter correction. *Physics in Medicine and Biology*, **56**, R85–112.

39. Metz CE, Atkins FB, and Beck RN. (1980). The geometric transfer function component for scintillation camera collimators with straight parallel holes. *Physics in Medicine and Biology*, **25**, 1059–70.

40. Tanaka M, Uehara S, Kojima A, et al. (2007). Monte Carlo simulation of energy spectra for 123I imaging. *Physics in Medicine and Biology*, **52**, 4409–25.

41. Budinger TF, Gullberg GT, Huesman RH. (1979). Emission computed tomography. Image reconstruction from projections: implementation and applications. **32**, 147–246.

42. Chang L-T. (1978). A method for attenuation correction in radionuclide computed tomography. *IEEE Transactions in Nuclear Sciences*, **NS-25**, 638–43.

43. Zaidi H, and Hasegawa BH. (2003). Determination of the attenuation map in emission tomography. *Journal of Nuclear Medicine*, **44**, 291–315.

44. Tsui BMW, Gullberg GT, Edgerton ER, et al. (1989). Correction of nonuniform attenuation in cardiac SPECT imaging. *Journal of Nuclear Medicine*, **30**, 497–507.

45. Tsui BMW, Zhao XD, Frey EC, et al. (1994). Quantitative single-photon emission computed-tomography—basics and clinical considerations. *Seminars in Nuclear Medicine*, **24**, 38–65.

46. Jaszczak RJ, Greer KL, Floyd CE, et al. Improved SPECT quantification using compensation for scattered photons. *Journal of Nuclear Medicine*, **25**, 893–900.

47. Ichihara T, Ogawa K, Motomura N, et al. (1993). Compton scatter compensation using the triple-energy window method for single- and dual-isotope SPECT. *Journal of Nuclear Medicine*, **34**, 2216–21.

48. King MA, Hademenos GJ, and Glick SJ. (1992). A dual-photopeak window method for scatter correction. *Journal of Nuclear Medicine*, **33**, 605–12.

49. Buvat I, Benali H, Toddpokropek A, et al. (1994). Scatter correction in scintigraphy—the state-of-the-art. *European Journal of Nuclear Medicine*, **21**, 675–94.

50. El Fakhri G, Maksud P, Kijewski MF, et al. (2000). Scatter and cross-talk corrections in simultaneous Tc-99m/I-123 brain SPECT using constrained factor analysis and artificial neural networks. *IEEE Transactions in Nuclear Sciences*, **47**, 1573–80.

51. Floyd CE, Jr, Jaszczak RJ, Greer KL, et al. (1985). Deconvolution of Compton scatter in SPECT.

Journal of Nuclear Medicine, **26**, 403–8.

52. Gilland DR, Tsui BMW, McCartney WH, et al. (1988). Determination of the optimum filter function for SPECT imaging. *Journal of Nuclear Medicine*, **29**, 643–50.

53. Yanch JC, Flower MA, and Webb S. (1988). A comparison of deconvolution and windowed subtraction techniques for scatter compensation in SPECT. *IEEE Transactions in Nuclear Sciences*, **7**, 13–20.

54. Frey EC, and Tsui BMW. (1996). A new method for modeling the spatially-variant, object-dependent scatter response function in SPECT. In: *1996 IEEE Nuclear Science Symposium Conference Record*, pp. 1082–6. Anaheim, CA.

55. Du Y, Tsui BMW, and Frey EC. (2006). Model-based compensation for quantitative I-123 brain SPECT imaging. *Physics in Medicine and Biology*, **51**, 1269–82.

56. Cao ZJ, Frey EC, and Tsui BMW. (1994). A scatter model for parallel and converging beam SPECT based on the Klein–Nishina formula. *IEEE Transactions in Nuclear Sciences*, **41**, 1594–600.

57. Riauka TA, and Gortel ZW. (1994). Photon propagation and detection in single-photon emission computed tomograph—an analytical approach. *Medical Physics*, **21**, 1311–22.

58. Beekman FJ, de Jong HWAM, and van Geloven S. (2002). Efficient fully 3-D iterative SPECT reconstruction with Monte Carlo-based scatter compensation. *IEEE Transactions in Medical Imaging*, **21**, 867–77.

59. Lazaro D, El Bitar Z, Breton V, et al. (2005). Fully 3D Monte Carlo reconstruction in SPECT: a feasibility study. *Physics in Medicine and Biology*, **50**, 3739–54.

60. El Fakhri G, Moore SC, Maksud P, et al. (2001). Absolute activity quantitation in simultaneous I-123/Tc-99m brain SPECT. *Journal of Nuclear Medicine*, **42**, 300–8.

61. Erlandsson K, Visvikis D, Waddington WA, et al. (1999). Dual radionuclide brain imaging with Tc-99m and I-123 with crosstalk corrections using multiple energy windows. *European Journal of Nuclear Medicine*, **26**, 1186.

62. Knesaurek K, and Machac J. (1997). Enhanced cross-talk correction technique for simultaneous dual-isotope imaging: a Tl-201/Tc-99m myocardial perfusion SPECT dog study. *Medical Physics*, **24**, 1914–23.

63. Links JM, Prince JL, and Gupta SN. (1996). A vector Wiener filter for dual-radionuclide imaging. *IEEE Transactions in Medical Imaging*, **15**, 700–9.

64. Neumann DR, and Chen EQ. (1992). Convolution-based method of energy spectral crosstalk correction for simultaneous, dual-isotope SPECT. *Radiology*, **185**, 176.

65. Yang JT, Yamamoto K, Sadato N, et al. (1997). Clinical value of triple-energy window scatter correction in simultaneous dual-isotope single-photon emission tomography with 123I-BMIPP and 201Tl. *European Journal of Nuclear Medicine*, **24**, 1099–106.

66. Du Y, Tsui BMW, and Frey EC. (2007). Model-based crosstalk compensation for simultaneous

Tc-99m/I-123 dual-isotope brain SPECT imaging. *Medical Physics*, **34**, 3530–43.

67. Pretorius PH, King MA, Pan TS, et al. (1988). Reducing the influence of the partial volume effect on SPECT activity quantitation with 3D modelling of spatial resolution in iterative reconstruction. *Physics in Medicine and Biology*, **43**, 407–20.

68. Soret M, Riddell C, Hapdey S, et al. (2001). Simultaneous attenuation and partial volume effect correction for SPECT I-123 dopamine receptor imaging. *Journal of Nuclear Medicine*, **42**, 57p.

69. Rousset O, Rahmim A, Alavi A, et al. (2007). Partial volume correction strategies in PET. *PET Clinics*, **2**, 235–49.

70. Erlandsson K, Buvat I, Pretorius PH, et al. (2012). A review of partial volume correction techniques for emission tomography and their applications in neurology, cardiology and oncology. *Physics in Medicine and Biology*, **57**, R119–59.

71. Meltzer CC, Zubieta JK, Links JM, et al. (1994). MRI-based correction for PET partial volume effects in the presence of heterogeneity in gray-matter radioactivity. *Journal of Nuclear Medicine*, **35**, P197.

72. Rousset OG, Ma Y, Evans AC. (1998). Correction for partial volume effects in PET: principle and validation. *Journal of Nuclear Medicine*, **39**, 904–11.

73. Du Y, Tsui BMW, Frey EC. (2005). Partial volume effect compensation for quantitative brain SPECT imaging. *IEEE Transactions in Medical Imaging*, **24**, 969–76.

74. Baete K, Nuyts J, Van Laere K, et al. (2004). Evaluation of anatomy based reconstruction for partial volume correction in brain FDG-PET. *NeuroImage*, **23**, 305–17.

75. Iida H, Law I, Pakkenberg B, et al. (2000). Quantitation of regional cerebral blood flow corrected for partial volume effect using O-15 water and PET: I. Theory, error analysis, and stereologic comparison. *Journal of Cerebral Blood Flow Metabolism*, **20**, 1237–51.

76. Acton PD, Meyer PT, Mozley PD, et al. (2000). Simplified quantification of dopamine transporters in humans using [99mTc]TRODAT-1 and single-photon emission tomography. *European Journal of Nuclear Medicine*, **27**:1714–18.

77. Habraken JB, Booij J, Slomka P, et al. (1999). Quantification and visualization of defects of the functional dopaminergic system using an automatic algorithm. *Journal of Nuclear Medicine*, **40**, 1091–7.

78. Baete K, Nuyts J, Van Paesschen W, et al. (2004). Anatomical-based FDG-PET reconstruction for the detection of hypo-metabolic regions in epilepsy. *IEEE Transactions in Medical Imaging*, **23**, 510–19.

79. Nuyts J, Baete K, Beque D, et al. (2005). Comparison between MAP and postprocessed ML for image reconstruction in emission tomography when anatomical knowledge is available. *IEEE Transactions in Medical Imaging*, **24**, 667–75.

80. Ogawa K, Ohmura N, Iida H, et al. (2009). Development of an ultra-high resolution SPECT system with a CdTe semiconductor detector. *Annals of Nuclear Medicine*, **23**, 763–70.

81. Takahashi Y, Miyagawa M, Nishiyama Y, et al. (2013). Performance of a semiconductor SPECT system: comparison with a conventional Anger-type SPECT instrument. *Annals of Nuclear Medicine*, **27**, 11–16.